Combination of isogeometric analysis and extended finite element in linear crack analysis

S. Shojaee[*1], M. Ghelichi[2] and E. Izadpanah[1]

[1]*Department of Civil Engineering, Shahid Bahonar University, Kerman, Iran*
[2]*Department of Civil Engineering, Graduate University Of Technology, Kerman, Iran*

Abstract.   This paper intends to present an application of isogeometric analysis in crack problems. An isogeometric formula is developed based on NURBS basis functions - enriched and adopted via X-FEM enrichment functions. The proposed method which is represented by the combination of the two above-mentioned methods, first by using NURBS functions models the geometry exactly and then by defining level set function on domain, identifies available discontinuity in elements. Additional DOFs are allocated to elements containing the crack and X-FEM enrichment functions enrich approximate solution. Moreover, a subelement refinement technique is used to improve the accuracy of integration by the Gauss quadrature rule. Finally, several numerical examples are illustrated to demonstrate the effectiveness, robustness and accuracy of the proposed method during calculation of crack parameters.

Keywords: isogeometric analysis; XFEM; crack analysis; NURBS; enrichment functions

1. Introduction

In the past decade, several numerical methods such as finite difference, boundary element and meshless methods have been innovated to remove the weaknesses of finite element method such as time consuming meshing process of the domain and large number of calculations. Because of low rate of convergence, finite difference method can hardly be used in solid mechanics in comparison with other methods. Notwithstanding the boundary element method (Cruse 1988) has many advantages in modeling discontinuities; we can't use it in nonlinear problems like plasticity or nonlinear geometry. Several meshless methods including element-free Galerkian method (EFG) (Belytschko 1994) were developed to remove difficulties of meshing, but those could not model the geometry exactly. Also, they have difficulties with integration and imposing boundary conditions and lack desired accuracy.

Dynamic crack propagation is a major challenge in numerical analysis. Because of the singularity existing in the crack tip, we have to use special elements abundantly which make the analysis slow. Also, the meshing must be correct to match with the crack propagation. One method which is regarded as the advantage of finite element and reduces the above problems is the X-FEM. This method is the product of using partition of unity in finite element method. The method

---

∗Corresponding author, Ph.D., E-mail: saeed.shojaee@mail.uk.ac.ir

of unity partition was proposed by Melenk and Babuska (1996). Oden *et al*. (1998), Duarte *et al*. (1998) Used partition of unity in finite element as a Generalized Finite Element Method (GFEM). The so-called X-FEM was primarily proposed by Belystchko and Black (1999). In their proposed method, discontinuities were modeled as a set of continuous and discontinuous functions called enrichment functions. In the proposed model, discontinuity was incompatible with the mesh. Moes *et al*. (1999) represented that we can use generalized Heaviside function to model cracks excluding crack tips.

Dolbow *et al*. (2001) modeled discontinuities and crack propagation trough frictional contact in 2D space. Duax *et al*. (2000) studied branched and intersecting cracks. Sukumar *et al*. (2001) proposed a methodology to model arbitrary holes and material interfaces, coupling the level set method with the extended finite-element method. The extended finite element in 3D space was run by Moes *et al*. (2002), Gravoil *et al*. (2002), Areias and Belystchko (2005). Moving phase boundary problems have been modeled by coupling the X-FEM with Level set function by Chessa *et al*. (2002), Ji *et al*. (2002), Zi and Belystchko (2003), Mergheim *et al*. (2005) studied cohesive crack problems. The Extended Finite Element Method uses the same basis and the same meshing method of classical finite element method to represent the geometry. This method has difficulty with modeling complex geometries. To improve modeling accuracy of the geometry and subsequently, to produce an accurate analysis, the isogeometric analysis is represented.

Recently, Hughes *et al*. (2005) proposed isogeometric analysis to improve the modeling accuracy of geometry in finite element method. Bazilevs, Hughes, and co-workers (2008, 2010) employed NURBS-based isogeometric analysis for the computation of laminar and turbulent flows as well as fluid–structure interaction in (2008, 2009). Hughes *et al*. (2008) studied the performance of NURBS-based isogeometric method for structural dynamics and wave propagation problems and proposed the efficient integration method for NURBS-based finite element. The mesh refinement and approximation continuity of isogeometric analysis was studied by Cottrell and Hughes (2007). Cottrell *et al*. (2006) also employed the isogeometric analysis in vibration problems. Benson *et al*. (2010) proposed a shear deformable shell formulation based on the isogeometric analysis methodology. Echter and Bischoff (2010) analyzed the efficiency and locking issues for NURBS-based analysis. The robustness of isogeometric discretizations was also investigated by Lipton *et al*. (2010). More recently, the isogeometric analysis was enhanced by T-splines with local refinement capability (Bazilevs *et al*. 2010, Döfel *et al*. 2010). Cottrell and co-workers (2009) represented details of isogeometric method. Also, dynamic analysis of fixed cracks in composites by the extended finite element method was represented by Motamedi (2010). Shojaee and Valizadeh (2012) studied NURBS-based isogeometric analysis for thin plate problems.

The XFEM with Lagrange basis functions cannot model complex geometries perfectly, but in isogeometric modeling with NURBS-based functions, it is capable of exact modeling of complex geometries and so represents more accurate solution. The XFEM needs classic finite element meshing that is considered quite time-consuming in the analysis process. But in isogeometric analysis the basic functions and so geometry of the problem have been modeled simply with knot vectors and control points.

Lately, Benson *et al*. (2010) introduced a generalized finite element formulation for arbitrary basis functions and combine the XFEM approach to linear fracture analysis with the higher-order NURBS based functions of isogeometric analysis. Lucker *et al*. (2011) presented a formula to combine XFEM and IGA and to study the convergence rate and relative error.

Table 1 Differences between XFEM and Xisogeometric

	XFEM	Xisogeometric
Meshing	Finite element mesh	Knot values in knot vectors
Geometry	Approximate	Exact
Assign variables	Node	Control point
Basis functions	Polynomials	NURBS basis
Kind of elements	Polygon	Polygon & Curve
Crack element integration	Triangulation	Local refinement

In this paper, we propose an isogeometric formulation based on NURBS basis functions (Xisogeometric), which have been enriched and adopted via XFEM enrichment functions and coupled with level set to solve the problems of fracture mechanics and reduce the weaknesses of numerical analysis methods. Several problems with linear and curved cracks are analyzed and then the crack propagation angle would be calculated. Some differences between XFEM and Xisogeometric are listed in Table 1.

2. Isogeometric analysis

The traditional finite element formulations is based on interpolation schemes with Lagrange, Legendre or Hermite polynomials to approximate geometry, physical field and its derivatives. This approach often requires a substantial simplification of the geometry, particularly for curved boundaries of the analysis domain. Generally, adaptive refinement of the discretized domain is applied to better approximate the boundary and to achieve sufficient convergence. The main idea of the isogeometric analysis is to apply the same interpolation scheme that is used accurately to describe the geometry for the approximation of the physical variables. Since NURBS-based functions have become a standard basis for describing and modeling the geometry in CAD and computer graphics, they are used to describe both of geometry and solution spaces.

2.1 NURBS basis function

NURBS are a generalization of piecewise polynomial B-splines curves. The B-spline basis functions are defined in parametric space on a knot vector Ξ. A knot vector in one dimension is a non-decreasing sequence of real numbers

$$\Xi = \left\{ \xi_1, \xi_2, ..., \xi_{n+p+1} \right\} \tag{1}$$

Where ξ_i is the ith knot, i is the knot index, $i = 1, 2,…, n+p+1$, p is the order of the B-spline, and n is the number of basis functions. The half open interval $[\xi_i, \xi_{i+1}]$ is called the ith knot span and it can have zero length since knots may be repeated more than one, and the interval $[\xi_i, \xi_{n+p+1}]$ is called a patch. In the isogeometric analysis, often open knot vectors are prefered. A knot vector is named open if it has $p+1$ repeating knots at the two ends. With a certain knot span, the B-spline basis functions are defined recursively as

$$N_{i,0}(\xi) = \begin{cases} 1 & if\ \xi_i \le \xi \le \xi_{i+1} \\ 0 & otherwise \end{cases} \tag{2}$$

and

$$N_{i,p}(\xi) = \frac{\xi - \xi_i}{\xi_{i+p} - \xi_i} N_{i,p-1}(\xi) + \frac{\xi_{i+p+1} - \xi}{\xi_{i+p+1} - \xi_{i+1}} N_{i+1,p-1}(\xi), \quad p = 1,\ 2,\ 3,\ \dots . \tag{3}$$

A B-spline curve of order p is defined by

$$C(\xi) = \sum_{i=1}^{n} N_{i,p}(\xi) T_i \tag{4}$$

where $N_{i,p}(\xi)$ is the ith B-spline basis function of order p and T are control points, given in d-dimensional space R^d. 1-D B-spline basis functions, built from open knot vectors, are interpolatory at the ends of parametric space. Fig. 1 shows the quadratic B-spline basis functions. In two dimensional space, B-spline basis functions are interpolatory at the corners of the patches. The non-uniform rational B-spline (NURBS) curve of order p is defined as

$$C(\xi) = \sum_{i=1}^{n} R_{i,p}(\xi) T_i \tag{5}$$

$$R_{i,p}(\xi) = \frac{N_{i,p}(\xi) w_i}{\sum_{i=1}^{n} N_{i,p}(\xi) w_i} \tag{6}$$

Here $R_{i,p}$ is the NURBS basis functions, T_i is the control point and w_i is the ith weight that must be non-negative. In the two dimensional parametric space $[0, 1]^2$, NURBS surfaces are constructed
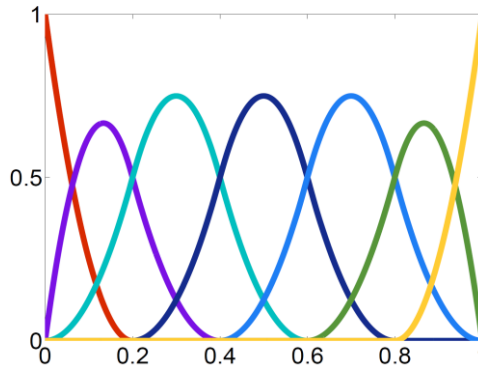

Fig. 1 Quadratic basis functions for an open knot vector $\Xi = \{0, 0, 0.2, 0.4, 0.6, 0.8, 1, 1.1\}$

by tensor product through knot vectors $\Xi=\{\xi_1, \xi_2, \ldots, \xi_{n+p+1}\}$ and $\Psi=\{\psi_1, \psi_2, \ldots, \psi_{m+q+1}\}$. It yields to

$$S(\xi,\psi) = \sum_{i=1}^{n}\sum_{j=1}^{m} R_{i,j}^{p,q}(\xi,\psi)T_{i,j} \tag{7}$$

where $T_{i,j}$ is the (i, j)-th of $n \times m$ control points, also called the control mesh. The interval $[\xi_1, \xi_{n+p+1}] \times [\psi_1, \psi_{m+q+1}]$ is a patch and $[\xi_i, \xi_{i+1}) \times [\psi_j, \psi_{j+1})$ is a knot span. $R_{i,j}^{p,q}(\xi,\psi)$ is the NURBS basis function in two dimensional space

$$R_{i,j}^{p,q}(\xi,\psi) = \frac{N_{i,p}(\xi)M_{j,q}(\psi)w_{i,j}}{W_{i,j}(\xi,\psi)} \tag{8}$$

and

$$W_{i,j}(\xi,\psi) = \sum_{i=1}^{n}\sum_{j=1}^{m} N_{i,p}(\xi)M_{j,q}(\psi)w_{i,j} \tag{9}$$

The derivative of $R_{i,j}^{p,q}(\xi,\psi)$ and $W_{i,j}(\xi, \psi)$ with respect to ξ is derived by simply applying the quotient rule to Eqs. (37) and (38)

$$\frac{\partial R_{i,j}^{p,q}(\xi,\psi)}{\partial\xi} = \frac{\dfrac{\partial N_{i,p}(\xi)}{\partial\xi}M_{j,q}(\psi)w_{i,j}W_{i,j}(\xi,\psi) - \dfrac{\partial W_{i,j}(\xi,\psi)}{\partial\xi}N_{i,p}(\xi)M_{j,q}(\psi)w_{i,j}}{(W_{i,j}(\xi,\psi))^2} \tag{10}$$

and

$$\frac{\partial W_{i,j}(\xi,\psi)}{\partial\xi} = \sum_{i=1}^{n}\sum_{j=1}^{m} \frac{\partial N_{i,p}(\xi)}{\partial\xi}M_{j,q}w_{i,j} \tag{11}$$

The domain of problem is divided into patches and each patch is divided into knot spans or elements. Patches play the role of sub-domains within which element types and material models are assumed to be uniform (Hughes *et al.* 2005). Nevertheless, many complicated domains can be represented by a single patch.

2.2 NURBS based isogeometric analysis formulation

Consider a 2-D linear elasticity problem with the presence of body force **b** and traction force $\overline{\mathbf{t}}$. Implementing the virtual displacement method, the following weak form equation is obtained

$$\int_{\Omega} \delta\boldsymbol{\varepsilon}^T \boldsymbol{\sigma} d\Omega - \int_{\Omega} \delta\mathbf{u}^T \mathbf{b} d\Omega - \int_{\Gamma_t} \delta\mathbf{u}^T \overline{\mathbf{t}} d\Gamma = 0 \tag{12}$$

where $\boldsymbol{\sigma}$ is the stress tensor and $\boldsymbol{\varepsilon}$ is the strain tensor. In isogeometric approach, the discretization is based on NURBS. Hence, the geometry and solution field are approximated as

$$\mathbf{x}(\xi,\psi) = \mathbf{RP} \qquad \xi,\psi \in \Omega_{patch} \tag{13}$$

$$\mathbf{u}^h(\xi,\psi) = \mathbf{Rd} \qquad \xi,\psi \in \Omega_{patch} \tag{14}$$

where $\Omega_{patch} = \left\{ (\xi,\psi) \middle| \xi \in \left[\xi_1,\xi_{n+p+1}\right], \psi \in \left[\psi_1,\psi_{m+q+1}\right] \right\}$. The matrix-form of $\mathbf{R}_{i,j}$ and $\mathbf{P}_{i,j}$ can be changed into vector-form by mapping from i, j subscripts to k by

$$k = i + (j-1)n, \qquad \text{with } k = 1,2,...,n.m \tag{15}$$

So, the control points are defined as

$$\mathbf{P} = (\mathbf{P}_{1,1}{}^x, \mathbf{P}_{1,1}{}^y, \mathbf{P}_{2,1}{}^x, \mathbf{P}_{2,1}{}^y, ..., \mathbf{P}_{n,m}{}^y)^T \tag{16}$$

The values of solution field at the control points, also called control variables, in the IGA formulation are displacements and can be arranged similar to the control points in a vector-form

$$\mathbf{d} = (\mathbf{d}_{1,1}{}^x, \mathbf{d}_{1,1}{}^y, \mathbf{d}_{2,1}{}^x, \mathbf{d}_{2,1}{}^y, ..., \mathbf{d}_{n,m}{}^y)^T \tag{17}$$

The matrix $\mathbf{R}$ is obtained from NURBS basis functions

$$\mathbf{R} = \begin{bmatrix} R_{1,1} & 0 & R_{2,1} & 0 & ... & R_{n,m} & 0 \\ 0 & R_{1,1} & 0 & R_{2,1} & ... & 0 & R_{n,m} \end{bmatrix} \tag{18}$$

Next, the stiffness matrix for a single patch is computed as

$$\mathbf{K}_{patch} = t \iint_{\hat{\Omega}} \mathbf{B}^T(\xi,\psi)\mathbf{DB}(\xi,\psi)|\mathbf{J}| d\hat{\Omega} \tag{19}$$

where t is the thickness, $\hat{\Omega}$ is the parametric space, $\mathbf{B}(\xi,\eta)$ is the strain-displacement matrix, and $\mathbf{J}$ is the Jacobian matrix which maps the parametric space to the physical space. $\mathbf{D}$ is the elastic material property matrix for plane stress state. The force vector on a single patch in the presence of body forces $\mathbf{b}$ and traction forces $\bar{\mathbf{t}}$ is obtained as

$$\mathbf{f} = \iint_{\hat{\Omega}} \mathbf{R}^T \mathbf{b} |\mathbf{J}| d\hat{\Omega} + \int_{\hat{\Gamma}} \mathbf{R}_b^T \bar{\mathbf{t}} |\mathbf{J}_b| d\hat{\Gamma} \tag{20}$$

where $\hat{\Gamma}$ is the traction boundary in the parametric space, $\mathbf{R}_b$ is the NURBS basis function evaluated on the traction boundary and $\mathbf{J}_b$ is the Jacobian that maps the traction boundary into a part of physical space boundary. The control variables can then be solved by the following discretized equilibrium equation

$$\mathbf{Kd} = \mathbf{f} \tag{21}$$

2.3 Imposition of essential boundary condition using Lagrange multiplier method

Due to the non-interpolating nature of NURBS basis functions, the properties of Kronecker Delta are not satisfied, and as a consequence, the imposition of essential boundary conditions needs special treatment. In this study, the Lagrange multiplier method is employed as a scheme for treatment of essential boundary conditions. Considering the problem of minimizing the total potential energy functional of stress field problem given by

$$\text{minimize}: \quad \pi = \frac{1}{2}t\int_{\Omega}\varepsilon^T \sigma d\Omega - t\int_{\Omega}u^T f_b d\Omega - \int_{\Gamma_N}u^T f_t d\Gamma$$

subject to:

$$g_1 = u - \overline{u}_1 \qquad on \ \Gamma_{D1}$$

$$g_2 = u - \overline{u}_2 \qquad on \ \Gamma_{D2} \tag{22}$$

$$.$$

$$.$$

$$.$$

$$g_m = u - \overline{u}_m \qquad on \ \Gamma_{Dm}$$

where $u=\{u_x, u_y\}^T$ is the degrees of freedom vector of system, $\overline{u}_i = \{\overline{u}_{xi}, \overline{u}_{yi}\}^T$ is the known value of displacement on Γ_{Di} boundary, and m is the number of Dirichlet boundaries. For the inclusion of the constraints into the variational problem, using Lagrange multiplier method, instead of seeking the minimum of π subjected to constraints, the Lagrange method seeks the stationary points that satisfies Eq. (23)

$$\text{minimize}: \quad \pi^* = \frac{1}{2}t\int_{\Omega}\varepsilon^T \sigma d\Omega - t\int_{\Omega}u^T f_b d\Omega - \int_{\Gamma_N}u^T f_t d\Gamma - \sum_{i=1}^{m}\int_{\Gamma_{Di}}\lambda_i(u - \overline{u}_i)d\Gamma \tag{23}$$

where λ_i is the Lagrange multiplier vector, corresponding to Γ_{Di} and is defined by

$$\lambda_i = \begin{Bmatrix} \lambda_{ix} \\ \lambda_{iy} \end{Bmatrix} \tag{24}$$

Now with approximation of λ_i and u, exact solution space will transform to approximate solution space,

$$u \cong u^h = Rd \tag{25}$$

where R and d are defined in Eqs. (17) and (18) respectively. Then Lagrange multiplier vector is discretized for obtaining matrix form of problem

$$\lambda_i = L_i \overline{\lambda}_i \qquad i = 1, 2...., m \tag{26a}$$

$$L_i = \begin{bmatrix} L_1^i & 0 & \cdots & \cdots & L_{nl}^i & 0 \\ 0 & L_1^i & \cdots & \cdots & 0 & L_{nl}^i \end{bmatrix} \tag{26b}$$

$$\overline{\lambda}_i = \left\{ \lambda_{1x}^i \quad \lambda_{1y}^i \quad ...... \quad \lambda_{nlx}^i \quad \lambda_{nly}^i \right\}^T \tag{26c}$$

Substituting Eqs. (25) and (26a) into Eq. (23), we have

$$\pi^* = \frac{1}{2}td^T \int_{\Omega} B^T DB \, d\Omega d - td^T \int_{\Omega} R^T f_b \, d\Omega - d^T \int_{\Gamma_N} R^T f_t \, d\Gamma - \sum_{i=1}^{m} \overline{\lambda}_i^T \int_{\Gamma_{Di}} L_i^T (Rd - \overline{u}_i) d\Gamma \tag{27}$$

The required solution of the problem is obtained by setting $\partial \pi^* / \partial d$ and $\partial \pi^* / \partial \bar{\lambda}_i$ to zero

$$t\int_{\Omega} B^T DB d\Omega d - t\int_{\Omega} R^T f_b \, d\Omega - \int_{\Gamma_N} R^T f_t \, d\Gamma - \sum_{i=1}^{m} \int_{\Gamma_{Di}} R^T L_i \, d\Gamma \bar{\lambda}_i = 0 \tag{28}$$

$$\int_{\Gamma_{Di}} L_i^T R \, d\Gamma \, d = \int_{\Gamma_{Di}} L_i^T \bar{u}_i \, d\Gamma \qquad i = 1, 2, ..., m \tag{29}$$

Then we obtain the system of algebraic equations

$$\begin{bmatrix} K & G \\ G^T & 0 \end{bmatrix} \begin{Bmatrix} d \\ \bar{\lambda} \end{Bmatrix} = \begin{Bmatrix} f \\ q \end{Bmatrix} \tag{30}$$

where

$$K = t\int_{\Omega} B^T DB \, d\Omega \tag{31a}$$

$$G = -\begin{bmatrix} G_1 & \cdots & \cdots & G_m \end{bmatrix} \quad , \quad G_i = \int_{\Gamma_{Di}} R^T L_i \, d\Gamma \tag{31b}$$

$$q = -\begin{bmatrix} q_1 & \cdots & \cdots & q_m \end{bmatrix} \quad , \quad q_i = \int_{\Gamma_{Di}} L_i^T \bar{u}_i \, d\Gamma \tag{31c}$$

$$f = t\int_{\Omega} R^T f_b \, d\Omega + \int_{\Gamma_N} R^T f_t \, d\Gamma \tag{31d}$$

$$\bar{\lambda} = \begin{Bmatrix} \bar{\lambda}_1 & \bar{\lambda}_2 & \cdots & \cdots & \bar{\lambda}_m \end{Bmatrix}^T \tag{31e}$$

3. The extended finite element method

Extended finite element method increases the accuracy and improves the convergence rate of FEM for singular problems. The basic concept of XFEM is to enrich the approximat space so that it be capable to reproduce certain features of the problems in particular discontinuities such as cracks or interfaces. Although it is a local version of the partition of unity finite element enrichment applied only in a certain local subdomain, it strongly relies on the development of extrinsic enrichments for crack simulations by a number of meshless methods such as EFG and Hp-clouds. Naturally, the first XFEM approximations were also developed for simulation of strong discontinuities in fracture mechanics. This was later extended to include weak discontinuity and interface problems. XFEM can be assumed to be a classical FEM capable of handling arbitrary strong and weak discontinuities. In the extended finite element method, first, the usual finite element mesh is produced. Then, by considering the location of discontinuities, a few degrees of freedom are added to the classical finite element model in selected nodes near to the discontinuities to provide a higher level of accuracy. Thus discontinuity is modeled without being considered in mesh explicitly. Assume that x be a point in $\mathfrak{R}^2$ (2D space) or $\mathfrak{R}^3$ (3D space) in finite element model and N be a nodal set of values like as $N_{el} = \{n_1, n_2, ..., n_m\}$, that m is number of
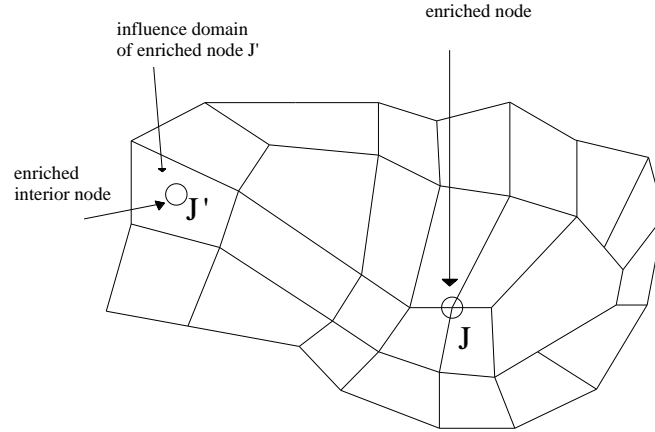
Fig. 2 Influence domains of an edge node *J* and an internal node *J'* in an arbitrary finite element mesh

nodes in one element, thus enriched approximate displacement for this point is defined as follows (Sukumar *et al*. 2001)

$$u^h(x) = u^{FEM} + u^{Enr} = \sum_{\substack{I \\ n_I \in \phi}} R_I(x)u_I + \sum_{\substack{J \\ n_J \in \phi^g}} R_J(x)Q(x)a_J \tag{32}$$

The first term is approximation of classical finite element to determine displacement, whereas the second term is enriched approximation to model the effect of existence of any discontinuity. u_I is vector of nodal DOFs in classical finite element, a_J is a set of additional DOFs to modeling discontinuity, R_I is basis function related to node *I* in classical finite element, $Q(x)$ is a discontinuous enrichment function and ϕ^g is a set of points defined as

$$\phi^g = \left\{ n_J : n_J \in \phi, \omega_J \cap \Omega_g \neq N \right\} \tag{33}$$

ω_J is the influence domain of basis function of N_J in node n_J, Ω_g is the domain depending on geometry of discontinuities such as surface or crack tip. Therefore, determination of enrichment function $Q(x)$, depends on type of discontinuity. Influence domain for node *J* is shown in Fig. 2.

To examine whether the Eq. (32) is an interpolation, the value of the field variable $u(x)$ on an enriched node *i* can be obtained as

$$u^h(x_i) = u_i + Q(x_i)a_i \tag{34}$$

Which means that it is not an interpolation and the nodal parameter u_i is not the real displacement value on the enriched node *i*. A simple remedy to this shortcoming is to shift the step function around the node of interest

$$u^h(x) = \sum_{\substack{I=1 \\ n_I \in \phi}}^{n} R_I(x)u_I + \sum_{\substack{J=1 \\ n_J \in \phi^g}}^{m} R_J(x)\big(Q(x) - Q(x_J)\big)a_J \tag{35}$$
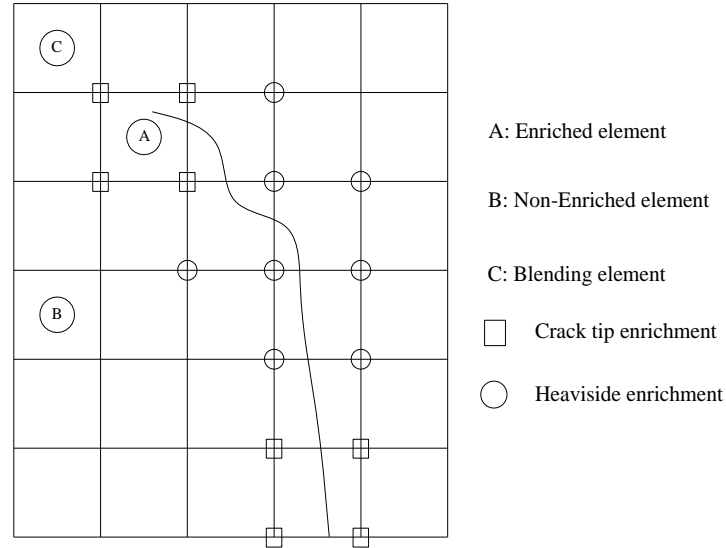
Fig. 3 Nodes selection for enrichment in XFEM

The enrichment function depending on the kind of discontinuity can change widely. But typical enrichment functions used in XFEM are the Heaviside functions, introduced by Krongauz and Belytschko (1998). This step function introduces a strong discontinuity in solution space and permits cracks to be incompatible with the mesh. The tip enrichment function define in polar coordinates (radius and angle), than the crack tip. There have been different approaches for the selection of nodes to be enriched by the Heaviside function. The procedure discussed in this section is only related to the Heaviside enrichment, and crack tip enrichments are separately applied to all nodes of the element that contains the crack tip. Fig. 3 illustrates the procedure of node selection for enrichment based on this formulation and also we can find three kinds of elements, enriched elements, nonenriched elements and blending elements.

4. Combining isogeometric with enrichment functions and level set

By introducing the XFEM enrichment functions in isogeometric analysis method and coupling with level set, the advantages of XFEM and isogeometric are combined. Thus, complex geometries can be represented exactly. Also, only by considering a few additional DOFs, accurate solutions are obtained in problems containing discontinuity or singularity and crack propagating problems can be analyzed.

4.1 Control points selection for enrichment

In the proposed method, we primarily select knot vectors and control points in such a way that we can be able to model the geometry exactly. Next, by defining level set function in any element, it can be determined whether this element splits with the crack or not. Split elements will enrich with Heaviside function and elements containing the tip of crack enrich with tip enrichment
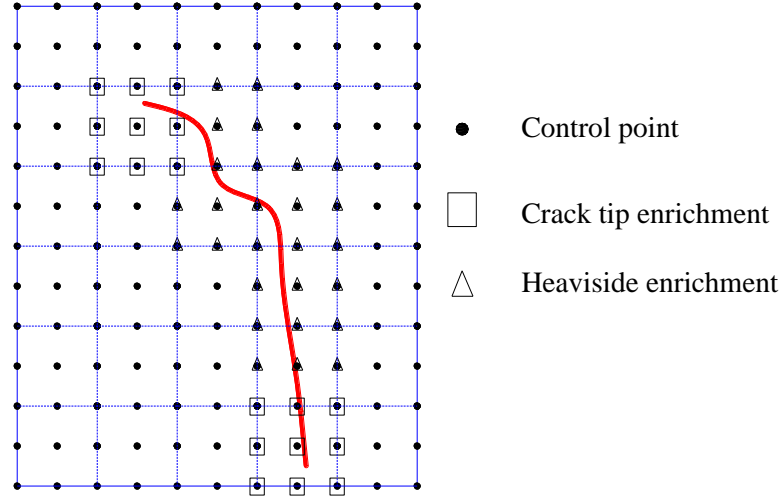
Fig. 4 Control points selection for enrichment in Xisogeometic

functions and additional DOFs allocated to control points belonging to these elements. For this proposed method, because always ther is at least a discountinuity in the problem, it is better to use more control points than what it's needed for modeling the geometry. In Fig. 4, control points in split elements are enriched with Heaviside enrichment function and are marked by triangle. Also, control points in crack tip elements are enriched with crack tip enrichment functions and are marked by square.

4.2 Crack modeling

4.2.1 Heaviside enrichment

Crack modeling process consists of two main parts, crack faces and crack tips. The difference between these parts in relation to stress is very high around the crack tips but not around crack faces whereas the displacement is discontinuous between above and below of crack faces. Therefore, it is obvious that it's essential to use two different types of enrichment functions to model these parts

$$u^h(x) = \sum_{j=1}^{n} R_j(x)u_j + \sum_{h=1}^{m} R_h(x)H(x)a_h +$$

$$\sum_{k=1}^{mt_1} R_k(x)\left(\sum_{L=1}^{mf} F_L^{\,1}(x)b^{L1}_{\;k}\right) + \sum_{k=1}^{mt_2} R_k(x)\left(\sum_{L=1}^{mf} F_L^{\,2}(x)b^{L2}_{\;k}\right) \tag{36}$$

n is the number of control points, m is the number of control points in split element, mt_1, mt_2 are the numbers of control points sets associated with in crack tips element 1 and 2, u_j is the displacement of control points (standard DOFs), a_h, $b_k^{\,1}$, $b_k^{\,2}$: are vectors containing additional DOFs for modeling tips and faces of crack. $H(\xi)$ is the generalized Heaviside function that is positive if x be at the top of crack and otherwise is negative. If e_n be the unit vector normalized to
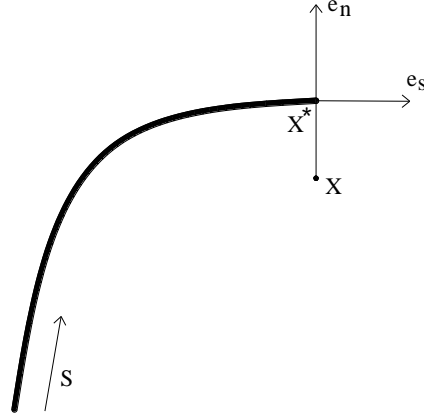
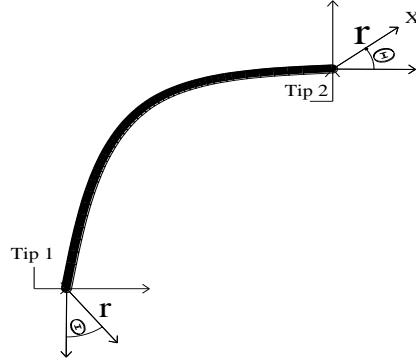Fig. 5 Normal and tangent unit vector in generalized Heaviside function

Fig. 6 Local polar axis defined in crack tips

crack direction and e_s be the unit vector tangent to crack direction and x^* be the nearest point to x (Fig. 6), Heaviside function is defined as

$$H(x) = \begin{cases} +1 & ;(x - x^*)e_n > 0 \\ -1 & ;(x - x^*)e_n < 0 \end{cases} \tag{37}$$

Additional degrees of freedom are considered for any degree of freedom which is belong to elements containing the crack. In a tip free crack, in the influence domain of an element, the control points which belong to this element will be enriched via the function Eq. (37).

4.2.2 Enrichment functions near the crack tip

The enrichment functions near the crack tip play an important role in modeling and calculating displacements and stresses especially in near crack tip. Take local polar axes (r, θ) in crack tips (Fig. 6), the displacement relations in near crack tip can be defined as

$$u_x = \frac{K_\mathrm{I}}{2G}\sqrt{\frac{r}{2\pi}}\left\{\cos(\theta/2)[\kappa - 1 + 2\sin^2(\theta/2)]\right\} + \frac{K_\mathrm{II}}{2G}\sqrt{\frac{r}{2\pi}}\left\{\sin(\theta/2)[\kappa - 1 + 2\cos^2(\theta/2)]\right\} \tag{38}$$

$$u_y = \frac{K_\mathrm{I}}{2G}\sqrt{\frac{r}{2\pi}}\left\{\sin(\theta/2)[\kappa+1-2\cos^2(\theta/2)]\right\} - \frac{K_\mathrm{II}}{2G}\sqrt{\frac{r}{2\pi}}\left\{\cos(\theta/2)[\kappa-1-2\sin^2(\theta/2)]\right\} \quad (39)$$

where K_I and K_II are the mode I and II stress intensity factors, respectively

$$K_\mathrm{I} = \lim_{\substack{r\to 0 \\ \theta=0}} \sigma_{yy}\sqrt{2\pi r} \quad (40)$$

$$K_\mathrm{II} = \lim_{\substack{r\to 0 \\ \theta=0}} \sigma_{xy}\sqrt{2\pi r} \quad (41)$$

and G is shear module and κ is

$$\kappa = \begin{cases} 3-4\nu & \text{for plane strain} \\ \dfrac{3-\nu}{1+\nu} & \text{for plane stress} \end{cases} \quad (42)$$

where ν is Poisson's ratio. Thus, we need to model the displacement space as well as Eq. (38) and Eq. (39). It is needed some functions that span all of possible displacements in these relations. We can find and select these functions in Dolbow (1999)

$$\{F_i(r,\theta)\}^4_{i=1} = \left\{\sqrt{r}\cos(\frac{\theta}{2}), \sqrt{r}\sin(\frac{\theta}{2}), \sqrt{r}\sin(\frac{\theta}{2})\sin(\theta), \sqrt{r}\cos(\frac{\theta}{2})\sin(\theta)\right\} \quad (43)$$

In these functions (r, θ) are calculated in local coordinates on crack tip. These functions are enrichment functions for crack tip. Enrichment is done for elements which crack tip is in their influence domain. Therefore, we need four functions to model crack tip. In plane stress and strain state, for each control point, we consider two degrees of motional freedom and no rotational degree. In each control point that needs the crack tip enrichment we must consider eight additional degrees of freedom to represent the effect of four functions in each direction. An approximate solution can then be constructed by blending the classical term and terms enriched with Heaviside and tip enrichment functions. The shifting techniques are used to transform approximate solution to interpolate approximate solution and more compatibility between enriched and non-enriched area

$$u^h(x) = \sum_{j=1}^{n} R_j(x)u_j + \sum_{h=1}^{m} R_h(x)\big(H(x)-H(\xi_h)\big)a_h +$$
$$\sum_{k=1}^{mt_1} R_k(x)\left(\sum_{L=1}^{mf}\big(F_L^1(x)-F_L^1(x_k)\big)b^{L1}_k\right) +$$
$$\sum_{k=1}^{mt_2} R_k(x)\left(\sum_{L=1}^{mf}\big(F_L^2(x)-F_L^2(x_k)\big)b^{L2}_k\right) \quad (44)$$

4.3 Numerical element integration

For numerical integration, the standard Gauss quadrature gives poor accuracy in the problems
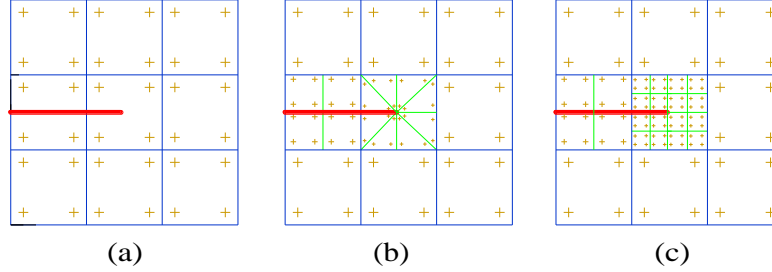
Fig. 7 Integration strategy. (a) initial; (b) almost polar in sub-cells in XFEM; (c) local refinement in Xisogeometric

with discontinuity or singularity. To overcome this issue, in the XFEM the elements containing the discontinuity are subdivided. Subdividing split elements into rectangular elements from crack direction and spread Gauss points in subelements and then it may be integrated. The best results were obtained by using almost polar integration (Laborde *et al*. 2005) for the element containing the crack tip enrichment. This integration method splits the quadrilaterals into triangles to concentrate the Gauss points near the tip and giving a regular distribution of integration points in terms of radius and angle (the polar coordinates relative to the tip), Fig. 7(b).

Generally, in isogeometric analysis, there are curved elements and it is difficult to use triangulation for crack element integration. Thus, it is necessary to modify the elements and quadrature points to accurately evaluate numerical integrations. An appropriate procedure is performed for elements located in crack tip. First, the parametric coordinate of crack tips (ξ, ψ) is determined using an inverse mapping from physical space. Then, by imposing local refinement to crack tip element, it is divided into subelements. Therefore, subelements have the same shape as original elements. Finally, spread Gauss points are divided into subelements according to Fig. 8. (c). It is essential to mention that these subelements are only generated for numerical integration.

5. Stress intensity factor evaluation, k

Knowledge of the displacements, strains, and stresses of a fracture model is useful, especially when interpreted by a post-processing program. However, these measures of a model's response consist of large amounts of tabulated data which are difficult to grasp as a whole. Stress intensity factors (SIFs) (Griffith *et al*. 1920, Irwin 1957) condense such data into an easily understood form and lend themselves more readily to analyze and design. Numerous techniques have been developed to compute SIFs, such as the displacement extrapolation method, the virtual crack extension method, and the interaction integral method. In the current work the last method is used. Specifically, the domain forms of contour interaction integral.

The interaction integral consists of superimposing auxiliary fields onto the actual fields produced by the solution of the boundary value problem. When the auxiliary fields are chosen in the proper form, the general 2D crack tip contour integral may be transformed into the contour interaction energy integral

$$I = \int_{\Gamma} (\sigma_{ik} \varepsilon_{ik}^{aux} \delta_{1j} - \sigma_{ij} u_{i,1}^{aux} - \sigma_{ij}^{aux} u_{i,1}) n_j d\Gamma \tag{45}$$

Where u_i^{aux}, ε_{ik}^{aux} and σ_{ij}^{aux} are, respectively, the auxiliary displacement, strain, and stress fields, the domain form of this interaction integral changes the evaluation of a line integral into the calculation of an integral over an area.

$$I = -\int_{\Gamma} (\sigma_{ik} \varepsilon_{ik}^{aux} \delta_{1j} - \sigma_{ij} u_{i,1}^{aux} - \sigma_{ij}^{aux} u_{i,1}) q_{,j} dA \tag{46}$$

Where q is a smooth scalar weighting function that is unity at the crack tip and becomes zero at the edge of the domain area. The interaction integral can be related to the SIFs as follows

$$I = \frac{2}{E \cosh^2(\pi\varepsilon)} [K_1 K_1^{aux} + K_2 K_2^{aux}] \tag{47}$$

where K_1^{aux} and K_2^{aux} are the auxiliary SIFs for the chosen auxiliary fields. With $K_1^{aux}=1$, $K_2^{aux}=0$ and with $I = I_1$, K_1 and K_2 can be obtained as

$$K_1 = \frac{E \cosh^2(\pi\varepsilon)}{2} I_1 \;,\; K_2 = \frac{E \cosh^2(\pi\varepsilon)}{2} I_2 \tag{48}$$

6. Crack propagation path

In this paper for predicting the crack propagation angle, the maximum hoop (circumferential) stress criterion is utilized. Stresses in this criterion for a crack under mixed mode loading are calculated in polar coordinates with the center on crack tip

$$\sigma_\theta = \frac{1}{\sqrt{2\pi r}} \cos^2(\frac{\theta}{2}) \left[K_I \cos(\frac{\theta}{2}) - 3K_{II} \sin(\frac{\theta}{2}) \right] \tag{49}$$

$$\tau_{r\theta} = \frac{1}{\sqrt{2\pi r}} \cos(\frac{\theta}{2}) \left[K_I \sin(\frac{\theta}{2}) \cos(\frac{\theta}{2}) + K_{II}(1 - 3\sin^2(\frac{\theta}{2})) \right] \tag{50}$$

The stress intensity factors in local coordinate system $x' - y'$, located in crack direction

$$K_I(\alpha) = \lim_{r\to 0} \sigma_\theta \sqrt{2\pi r} = \cos^2 \frac{\alpha}{2} \left[K_I \cos \frac{\alpha}{2} - 3K_{II} \sin \frac{\alpha}{2} \right] \tag{51}$$

$$K_{II}(\alpha) = \lim_{r\to 0} \tau_{r\theta} \sqrt{2\pi r} = \cos \frac{\alpha}{2} \left[K_I \sin \frac{\alpha}{2} \cos \frac{\alpha}{2} + K_{II}(1 - 3\sin^2 \frac{\alpha}{2}) \right] \tag{52}$$

Crack propagation angle is calculated such a way that the value of σ_θ would be maximum

$$\frac{\partial \sigma_\theta}{\partial \theta} = 0 \Rightarrow \alpha = 2 \tan^{-1} \left[\frac{1}{4} \frac{K_I}{K_{II}} \pm \frac{1}{4} \sqrt{(\frac{K_I}{K_{II}})^2 + 8} \right] \tag{53}$$
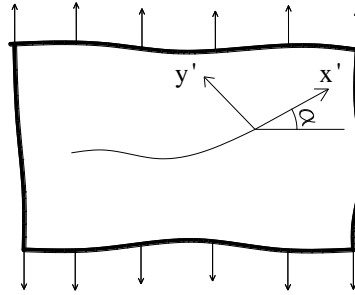
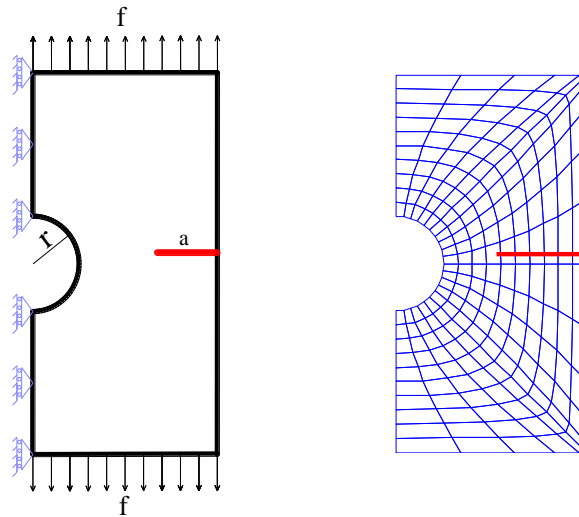Fig. 8 Local coordinate system located in crack tip and mixed mode loading representation

Fig. 9 Geometry of the plate with edge crack

So, to predict the crack propagation path, in each step of crack growth, it is quite sufficient to calculate stress intensity factors in mode I , II and then with the Eq. (53), the crack propagation angle is calculated, (Fig. 8).

7. Numerical examples

In this section, the validity and the accuracy of proposed approach are demonstrated. Different numerical examples with various conditions are presented. The results obtained by the proposed Xisogeometric analysis are also compared with XFEM solutions.

7.1 Tension plate with a hole and edge crack under distributed loading

In this example, a tension plate is considered which has a central hole with two cracks on the left and right edge. Because of symmetry, only half of the plate for analyzing is considered as
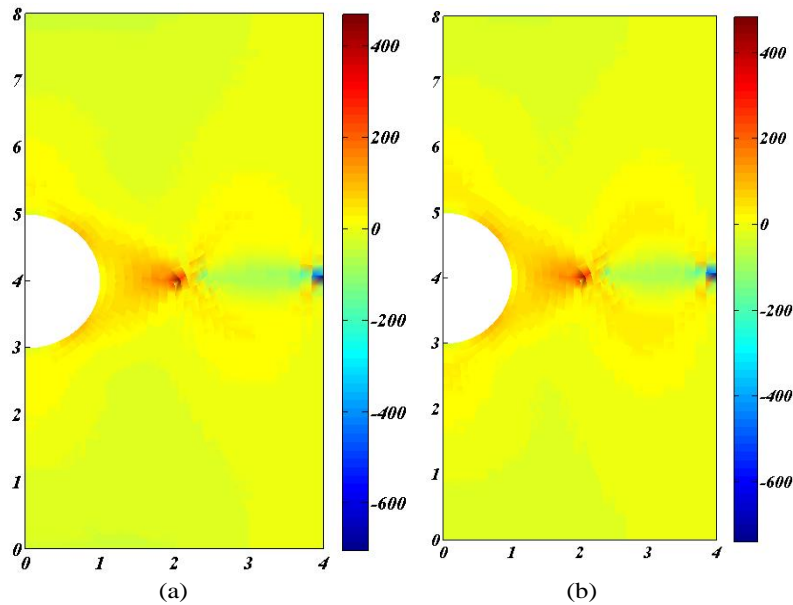
Fig. 10 Stress in *X* direction (a) XFEM (b) Xisogeometric

Table 2 Comparison between results of XFEM and Xisogeometric method

Method	Number of DOFs	Maximum of displacement	Maximum of stress (in crack tip)	Stress intensity factor	Time of analysis (s)
XFEM	3600	0.72	674	1.164	267
Xisogemetric	1800	0.72	682	1.167	28

shown in Fig. 9. The left edge is fixed in *X* direction and other sides are free. The half of the plate length is 8 and the width is 4. Also, the radius of hole is 1 and the length of the crack is 2. The magnitude of the distributed loading (*f*) is 100. The comparison between the results of XFEM and Xisogeometric in this problem has been represented in Table 2. In Fig. 11, the distribution contours of stress in *X* direction for both XFEM and Xisogeometric is presented.

From Table 2, it can be concluded that Xisogeometric results are very close to XFEM even if the lower number of DOFs were used. The accuracy of Xisogeometric is higher than XFEM and it represents the fact that the proposed method for numerical integration in crack elements is acceptable. Also, time of Xisogeometric analysis is very lower than XFEM and it is a very fast method.

7.2 Plate with a central crack under concentrated loading

The next example refers to a rectangular plate with rigidly fixed bottom edge in the *X* and *Y* direction under concentrated loading. The length of plate (*b*) is 10 and its width (*L*) and thickness are 5 and 1, respectively. A horizontal concentrated loading *f*=100 is applied at the top left corner, as shown in Fig. 11. Young's modulus and Poisson ratio are considered 1500 and 0.25, respectively. The length of the crack (*a*) is 2. The distribution of Gauss quadrature points near the crack is shown in Fig. 12.
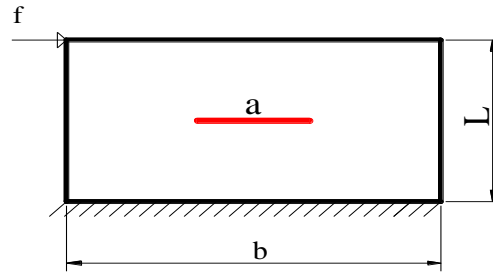
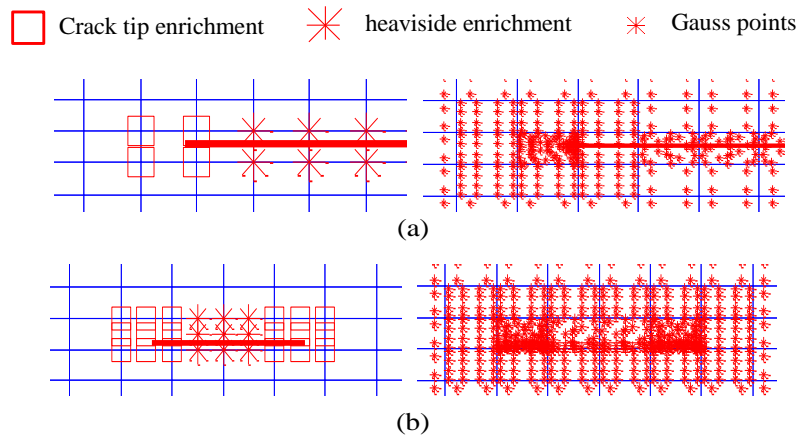Fig. 11 Geometry of the plate with a central crack

Fig. 12 Selection of enrichment and position of Gauss points around the edge crack (a) XFEM (b) Xisogeometric
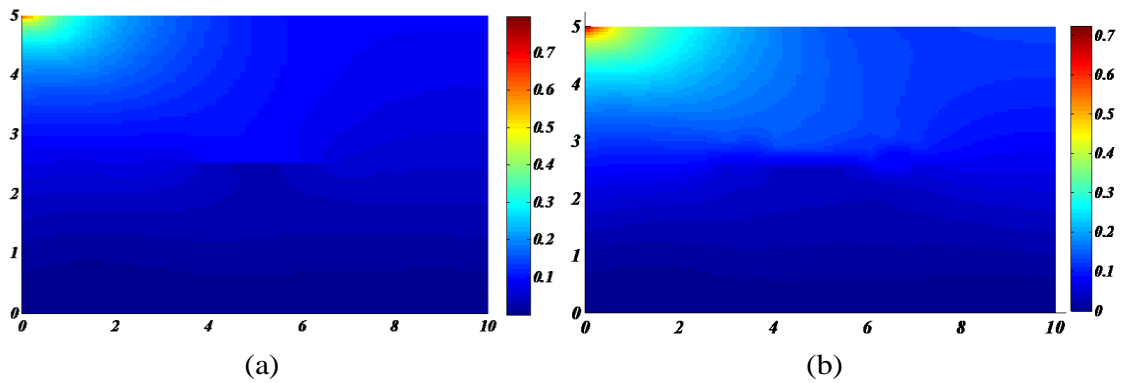

Fig. 13 Displacement in *X* direction (a) XFEM , (b) Xisogeometric

Table 3 Comparison between results of XFEM and Xisogeometric method

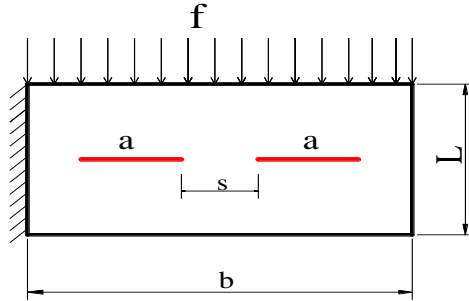| Method	Number of DOFs	Maximum of displacement	Maximum of stress (in crack tip)	Stress intensity factor	Time of analysis (s)
XFEM	12800	0.74	387	1.045	288
Xisogemetric	4000	0.74	382	1.037	34

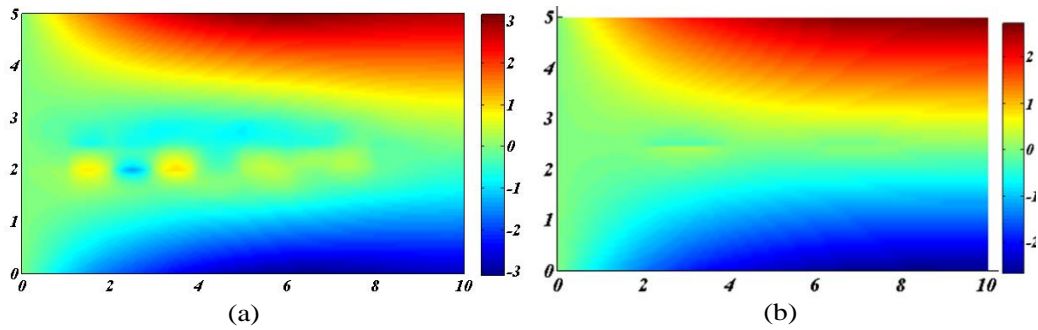Fig. 14 Modeling of the plate with double internal crack

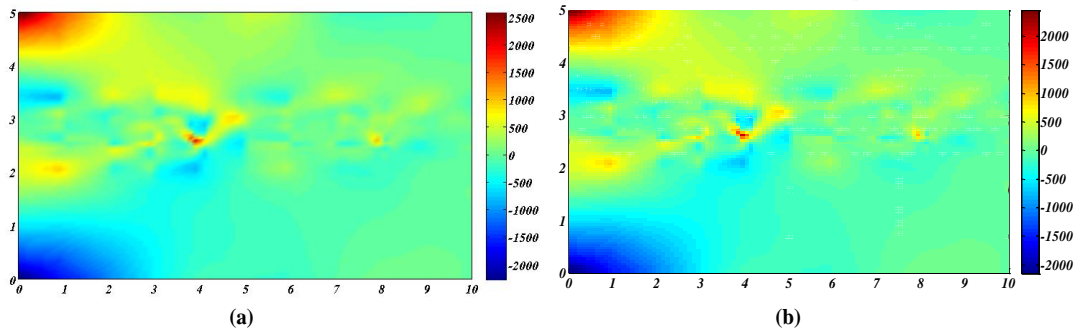Fig. 15 Displacement in *X* direction (a) XFEM (b) Xisogeometric

Fig. 16 Stress in X direction (a) XFEM (b) Xisogeometric

In Fig. 13, the distribution contours of displacement is shown in *X* direction using XFEM and Xisogeometric. In Table 3, remarkable agreements can be observed between results of XFEM and Xisogeometric. In order to present the computational efforts involved in numerical simulation, the time of analysis also is given in Table 3.

7.3 Plate with double internal crack under distributed loading

In this example, a rectangular plate with rigidly fixed left edge in the *X* and *Y* direction under distributed loading in plain strain is modeled with Xisogeometric method and XFEM. The length of plate (*b*) is 10 and width (*L*) and thickness are 5 and 1, respectively. A vertical distributed
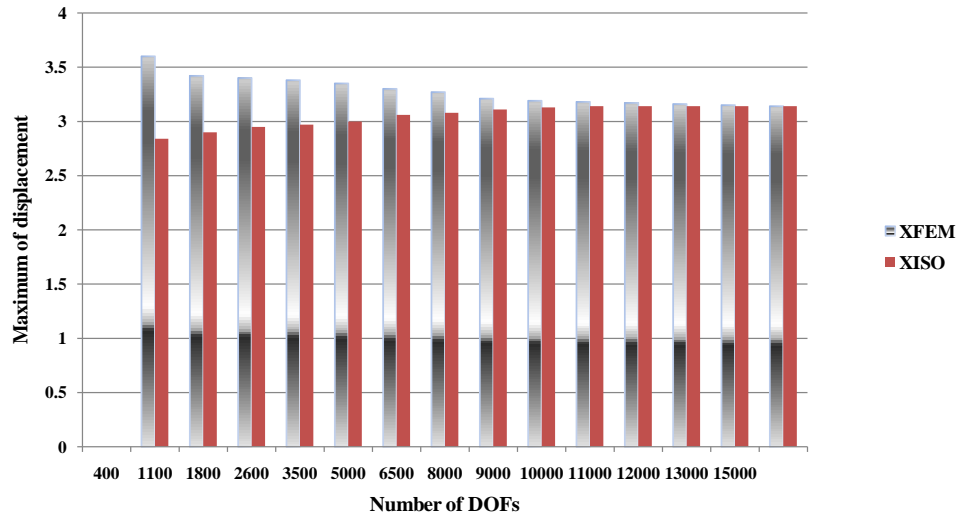
Fig. 17 Convergence diagram of XFEM and XISO

Table 4 Comparison between results of XFEM and Xisogeometric method

Method	Number of DOFs	Maximum of displacement	Maximum of stress (in crack tip)	Stress intensity Factor (Average)	Time of analysis (s)
XFEM	15000	3.14	2561	0.782	303
Xisogemetric	5000	3.14	2542	0.777	31

loading (*f*) is applied at the top edge as shown in Fig. 14. The magnitude of *f* is considered 100. Young's modulus and Poisson ratio are considered 1500, 0.25 respectively. The length of the each crack (*a*) and distance between them are 2.

The distribution contours of displacement and stress in *X* direction for both XFEM and Xisogeometric are shown in Fig. 15 and Fig. 16.

The accuracy of proposed method in comparison with XFEM is shown in Fig. 18. It can be seen from this example in Table 4 that because of the two cracks, Xisogeometric analysis results in better time of analysis. Relatively complete agreement can be observed between the XFEM and Xisogeometric method in maximum of displacements, maximum of stresses and average of stress intensity factors.

7.4 Disk with a hole and curved crack

This example is a tension disk with a central hole and two asymmetric curved cracks on the left and right internal edges as shown in Fig. 18. The internal and external radiuses are considered 2 and 4, respectively. The magnitude of tension loading (*f*) is 100. Young's modulus of material and Poisson ratio are 1500 and 0.25, respectively.

In Figs. 20 and 21, the distribution contours of displacement and stress in *Y* direction using Xisogeometric and XFEM are indicated. In Table 5, good agreements can be observed in the results from XFEM and Xisogeometric. This example adequately demonstrates the capability of the proposed approach in modeling problems with curved cracks.
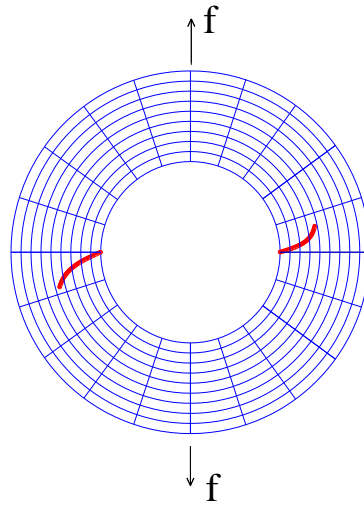
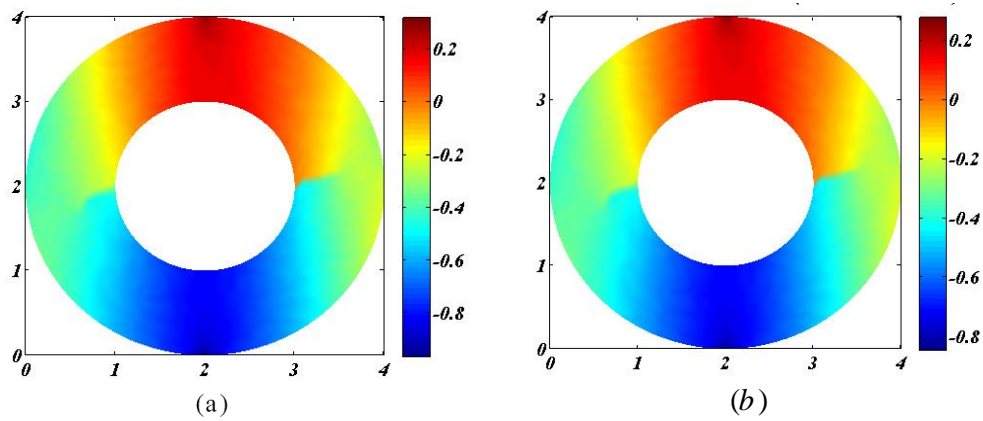Fig. 18 Geometry of the disc with double edge crack

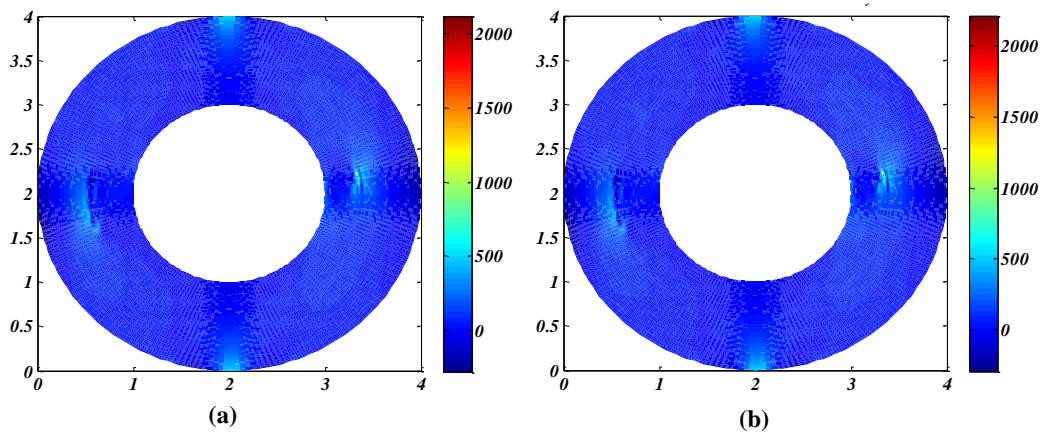Fig. 19 Displacement in *Y* direction (a) Xisogeometric, (b) XFEM

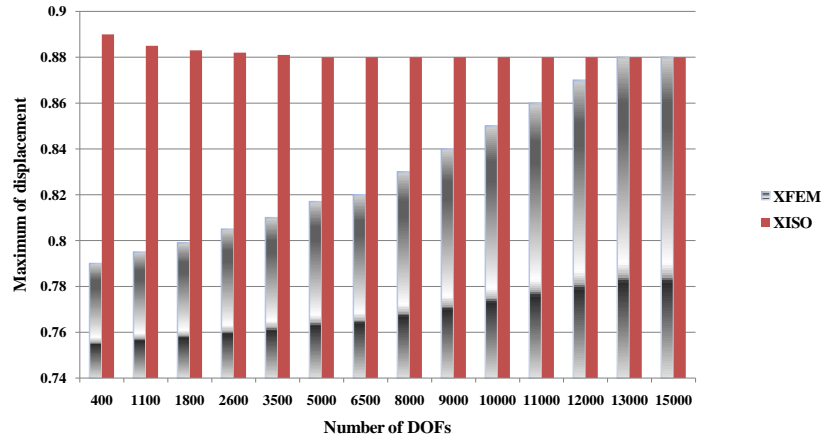Fig. 20 Stress in *Y* direction (a) Xisogeometric, (b) XFEM

Fig. 21 Convergence diagram of XFEM and XISO

Table 5 Comparison between results of XFEM and Xisogeometric method

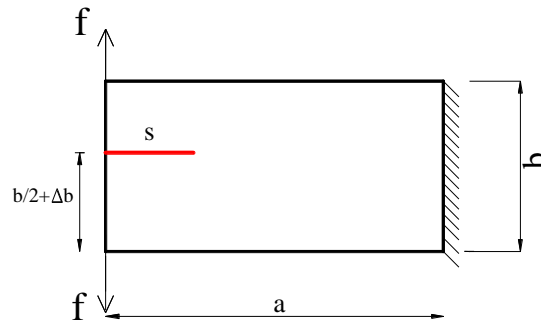| Method	Number of DOFs	Maximum of displacement	Maximum of stress (in crack tip)	Time of analysis (s)
XFEM	14000	0.88	2221	257
Xisogemetric	4000	0.88	2246	38

Fig. 22 Double cantilever beam with an edge crack

It can be seen that the convergence value is 0.88, so the proposed method would reach to this value much quicker than extended finite element method. Thus, using the proposed method, crack analyzing problems will be done with the minimum number of DOFs and also analysis duration will decrease remarkably.

7.5 Double cantilever beam with an edge crack

In this example, a crack in a double cantilever beam propagates in a quasi-static state. As shown in Fig. 22, the geometry and loading specifications are: a=60 mm, b=20 mm, f=1.0×10^5 N, E=3×10^7 N/mm^2, v =0.3. An initial crack with the length of s=20 mm is placed slightly off the mid-plane (ΔS=0.14 mm). The mixed mode SIFs are computed using the domain form of the
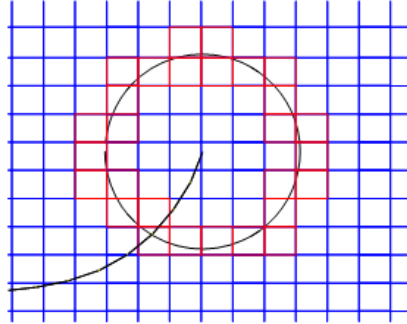
Fig. 23 The near crack tip integration domain for SIFs computation

Table 6 Mixed mode SIFs and crack inclination angle in the local crack tip and global coordinate systems for each step of crack propagation

| Step	K_I	K_II	$\theta_c(°)$	$\alpha(°)$
1	2032204.81	-5166.41	2.0181	2.0181
2	300549.35	-7827.18	2.9898	5.0079
3	312732.60	-9010.08	3.2951	8.3030
4	328327.78	-15221.38	5.2865	13.5895
5	344832.20	-26711.72	8.7555	22.3450
6	369742.88	-30384.36	9.2726	31.6176
7	408041.16	-46464.16	12.6748	44.2924
8	491816.86	-61558.34	13.8517	58.1441
9	563412.67	-47398.67	9.4860	67.6301
10	760009.40	-51844.11	7.7337	76.3638
11	939907.63	-36301.03	4.4104	79.7742
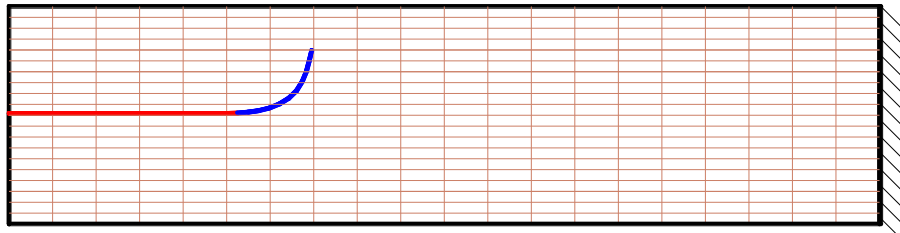
Fig. 24 Initial crack path as a red line and crack propagation path as a blue curve

interaction integral in a circular domain with radius $r_j=0.15 \times s$. Fig. 23 shows the selected elements for the domain integration in computing SIFs. It should be emphasized that the control points and elements distribution are fixed in the whole crack propagation process without any re-meshing.

To predict the crack propagation path with the Xisogeometric method, eleven steps are considered with a crack increment of length 1 mm. The resulting path (Fig. 24) is very similar to the crack growth path reported by Sukumar (2003) where XFEM was used to simulate crack propagation (without mentioning the exact value of). In Table 6, mixed mode SIFs and crack inclination angle is presented in the local crack tip and global coordinate systems.

8. Conclusions

The present paper introduced isogeometric modeling of cracks in fracture mechanics. The Xisogeometric formulation was developed through implementation of the enrichment functions to approximate the displacement fields of elements located on crack tip. A modified technique was used for the improvement of the integration accuracy by the Gauss quadrature rule.

The applicability of proposed formulation was finally demonstrated through several numerical examples. The Xisogeometric modeling decreases the time of analysis and can analyze the complex geometries with a coarse mesh incompatible with the crack. The simulation of the deformation as well as the distribution of stresses was shown and the results were compared with those obtained by the XFEM analysis. The results clearly indicate that the proposed method can efficiently be used to analyze crack problems and predict the crack path.

References

Areias, P.M.A. and Belytschko, T. (2005), "Analysis of three-dimensional crack initiation and propagation using the extended finite element method", *Int. J. Numer. Method. Eng.*, **63**(10), 760-788.

Bazilevs, Y. and Hughes, T.J.R. (2008), "NURBS-based isogeometric analysis for the computation of flows about rotating components", *Comput. Mech.*, **43**(5-8), 143-150.

Bazilevs, Y. and Akkerman, I. (2010), "Large eddy simulation of turbulent Taylor–Couette flow using isogeometric analysis and the residual-based variational multiscale method", *J. Comput. Phys.*, **229**(9), 3402-3414.

Bazilevs, Y., Calo, V.M,, Zhang. Y, and Hughes, T.J.R. (2008), "Isogeometric fluid–structure interaction analysis with applications to arterial blood flow", *Comput. Mech.*, **38**(1), 310-322.

Bazilevs, Y., Gohean, J.R,, Hughes, T.J.R., Moser, R.D. and Zhang, Y. (2009), "Patient-specific isogeometric fluid–structure interaction analysis of thoracic aortic blood flow due to implantation of the Jarvik 2000 left ventricular assist device", *Comput. Methods Appl. Mech. Eng.*, **198**(5), 3534-3550.

Bazilevs, Y., Calo, V.M., Cottrell, J.A., Evans, J.A., Hughes, T.J.R., Lipton, S., Scott, M.A. and Sederberg, T.W. (2010), "Isogeometric analysis using T-splines", *Comput. Methods Appl. Mech. Eng.* **199**(4), 229-263

Belytschko, T., Lu, Y.Y. and Gu, L. (1994), "Element-free Galerkin methods", *Int. J. Numer. Methods Eng.*, **37**(2), 229-256.

Belytschko, T. and Black, T. (1999). "Elastic crack growth in finite elements with minimal remeshing", *Int. J. Numer. Methods Eng.*, **45**(5), 601- 620.

Benson, D.J., Bazilevs, Y., Hsu, M.C. and Hughes, T.J.R. (2010), "Isogeometric shell analysis: the Reissner–Mindlin shell", *Comput. Methods Appl. Mech. Eng.*, **199**(5-8), 276-289.

Benson, D.J., Bazilevs, Y., Luycker, E.D., Hsu, M.C., Scott, M., Hughes, T.J.R. and Belytschko, T. (2010), "A generalized finite element formulation for arbitrary basis functions: From isogeometric analysis to XFEM", *Int. J. Numer. Methods Eng.*, **83**(6), 765-785.

Chessa, J., Smolinski, P. and Belytschko, T. (2002), "The extended finite element method (XFEM) for solidification problems", *Int. J. Numer. Methods Eng.*, **53**(8), 1959-1977.

Cottrell, J.A., Hughes, T.J.R. and Reali, A. (2007), "Studies of refinement and continuity in isogeometric structural analysis", *Comput. Methods Appl. Mech. Eng.*, **196**(41-44), 4160-4183.

Cottrell, J.A., Reali, A., Bazilevs, Y. and Hughes, T.J.R. (2006), "Isogeometric analysis of structural vibrations", *Comput. Methods Appl. Mech. Eng.*, **195**(41-43), 5257-5296.

Cottrell, J.A., Hughes, T.J.R. and Bazilevs, Y. (2009), *Isogeometric analysis: toward integration of CAD and FEA*, WILEY, Singapore.

Cruse, T. (1988), *Boundary Element Analysis in Computational Fracture Mechanics*, Kluwer, Dordrecht.

Dolbow, J., Mo,Y.N. and Belytschko, T. (2001), "An extended finite element method for modeling crack growth with frictional contact", *Comput. Methods Appl. Mech. Eng.*, **190**(1), 6825-6846.

Dolbow, J. (1999), "An extended finite element method with discontinuous enrichment for applied mechanics", *Theor. Appl. Mech.*, Ph. D. Thesis, Northwestern University, Evanston, IL, USA.

Duarte, C.A., Babuška, I. and Oden, J.T. (1998), "Generalized finite element methods for three dimensional structural mechanics problems", *Proceeding of the International Conference on Computational Science*, *Atlanta, GA. Tech. Science Press*, **1**(1), 53-58.

Duax, C., Mo, Y.N., Dolbow, J., Sukumar, N. and Belytschko, T. (2000), "Arbitrary cracks and holes with the extended finite element method", *Int. J. Numer. Methods Eng.*, **48**(3), 1741-1760.

Döfel, M.R., Jüttler, B. and Simeon, B. (2010), "Adaptive isogeometric analysis by local hrefinement with T-splines", *Comput. Meth. Appl. Mech. Eng.*, **199**(2), 264-275.

Echter, R. and Bischoff, M. (2010), "Numerical efficiency, locking and unlocking of NURBS finite elements", *Comput. Methods Appl. Mech. Eng.*, **199**(5), 374-382.

Gravouil, A., Mo, Y.N. and Belytschko, T. (2002), "Non-planar 3D crack growth by the extended finite element and the level sets-Part II: level set update", *Int. J. Numer. Methods Eng.*, **53**(3), 2569-2586.

Griffith, A.A., Lond, R. and Ser, A. (1920), "The phenomena of rapture and flow in solids", **221**, 163-198.

Hughes, T.J.R., Cottrell, J.A. and Bazilevs, Y. (2005), "Isogeometric analysis: CAD, finite elements, NURBS, exact geometry and mesh refinement", *Comput. Methods Appl. Mech. Eng.*, **194**(1), 4135-4195.

Hughes, T.J.R., Reali, A. and Sangalli, G. (2008), "Duality and unified analysis of discrete approximations in structural dynamics and wave propagation: comparison of p-method finite elements with k-method NURBS", *Comput. Methods Appl. Mech. Eng.*, **197**(49-50), 4104-4124.

Hughes, T.J.R., Reali, A. and Sangalli, G. (2010), "Efficient quadrature for NURBS-based isogeometric analysis", *Comput. Methods Appl. Mech. Eng.*, **199**(5-8), 301-313.

Irwin, G.R. (1957), "Analysis of stresses and strains near the end of a crack traversing a plate", *J. Appl. Mech.*, **24**, 361-364.

Ji, H., Chopp, D. and Dolbow, J. (2002), "A hybrid extended finite element/level set method for modeling phase transformations", *Int. J. Numer. Methods Eng.*, **54**(8), 1209-1233.

Krongauz, B.T. (1998), "EFG approximation with discontinuous derivatives", *Int. J. Numer. Methods Eng.*, **41**(7), 1215-1233.

Laborde, P., Pommier, J., Renard, Y. and Salaün, M. (2005), "High-order extended finite element method for cracked domains", *Int. J. Numer. Methods Eng.*, **64**(3), 354-381.

Lipton, S., Evans, J.A., Bazilevs, Y., Elguedj, T. and Hughes, T.J.R. (2010), "Robustness of isogeometric structural discretizations under severe mesh distortion", *Comput. Meth. Appl. Mech. Eng.*, **199**(9), 357-373.

Luycker, E.D., Benson, D.J., Belytschko, T., Bazileves, Y. and Hsu, M.C. (2011), "X-FEM in isogeometric analysis for linear fracture mechanics", *Int. J. Numer. Methods Eng.*, **87**(6), 541-565.

Melenk, J.M. and Babuška, I. (1996), "The partition of unity finite element method: basic theory and applications", *Comput. Methods Appl. Mech. Eng.*, **139**(1-4), 289-314.

Mergheim, J., Kuhl, E. and Steinmann, P. (2005), "A finite element method for the computational modeling of cohesive cracks", *Int. J. Numer. Methods Eng.*, **63**(2), 276-289.

Motamedi, D. and Mohammadi, S. (2010), "Dynamic analysis of fixed cracks in composites by the extended finite element method", *Eng. Fract. Mech.*, **77**(17), 3373-3393.

Mo, Y.N., Dolbow, J. and Belytschko, T. (1999), "A finite element method for crack growth without remeshing", *Int. J. Numer. Methods Eng.*, **46**(1), 131-150.

Mo, Y.N., Gravouil, A. and Belytschko, T. (2002), "Non-planar 3D crack growth by the extended finite element and the level sets-Part I: mechanical model", *Int. J. Numer. Methods Eng.*, **53**(11), 2549-2568.

Oden, J.T., Duarte, C.A. and Zienkiewicz, O.C. (1998), "A new cloud-based hp finite element method", *Comput. Methods Appl. Mech. Eng.*, **153**(1-2), 117-126.

Shojaee, S. and Valizadeh, N. (2012), "NURBS-based isogeometric analysis for thin plate problems", *Struct. Eng. Mech.*, **5**(41), 617-632.

Sukumar, N., Chopp, D.L., Mo, Y.N. and Belytschko, T. (2001), "Modeling holes and inclusions by level

sets in the extended finite element method", *Comput. Methods Appl. Mech. Eng*., **190**(46-47), 6183-6200.
Sukumar, N. and Prévost, J.H. (2003), "Modeling quasi-static crack growth with the extended finite element method. Part II: Numerical applications", *Int. J. Solids Struct*., **40**(26), 7539-7552.
Zi, G. and Belytschko, T. (2003), "New crack-tip elements for XFEM and applications to cohesive cracks", *Int. J. Numer. Meth. Eng*., **57**(15), 2221-2240.